

# Sampling and Reconstruction of Bandlimited Signals with Multi-Channel Time Encoding

Karen Adam, *Student Member, IEEE*, Adam Scholefield, *Member, IEEE*, Martin Vetterli, *Fellow, IEEE*

**Abstract**—Sampling is classically performed by recording the amplitude of the input at given time instants; however, sampling and reconstructing a signal using multiple devices in parallel becomes a more difficult problem to solve when the devices have an unknown shift in their clocks.

Alternatively, one can record the times at which a signal (or its integral) crosses given thresholds. This can model integrate-and-fire neurons, for example, and has been studied by Lazar and Tóth under the name of “Time Encoding Machines”. This sampling method is closer to what is found in nature.

In this paper, we show that, when using time encoding machines, reconstruction from multiple channels has a more intuitive solution, and does not require the knowledge of the shifts between machines. We show that, if single-channel time encoding can sample and perfectly reconstruct a  $2\Omega$ -bandlimited signal, then  $M$ -channel time encoding can sample and perfectly reconstruct a signal with  $M$  times the bandwidth. Furthermore, we present an algorithm to perform this reconstruction and prove that it converges to the correct unique solution, in the noiseless case, without knowledge of the relative shifts between the machines. This is quite unlike classical multi-channel sampling, where unknown shifts between sampling devices pose a problem for perfect reconstruction.

**Keywords**—Bandlimited signals, sampling methods, signal reconstruction.

## I. INTRODUCTION

Almost all current sampling theories represent a signal using (time, amplitude) pairs. However, this is quite different from the way encoding is done in nature, where processes have undergone millions of years of evolution. More precisely, when a neuron takes an input, it outputs a series of action potentials—the *timings* of which encode the original input.

In this paper, we consider time encoding. The output of a time encoding machine (TEM) [1] is not a series of (time, amplitude) pairs as in classical sampling, but rather a series of signal-dependent time points, which is reminiscent of the output of spiking neurons. The resemblance is highlighted in Fig. 1 where we depict the outputs of three different encoding schemes: encoding using classical sampling, using a leaky integrate-and-fire neuron and using a time encoding machine.

Classical sampling and reconstruction has been revisited frequently with extensions proposed along two axes: the sampling setup and the signal class. For example, the traditional

Shannon-Nyquist-Kotelnikov sampling setup [2,3] has been extended to setups where samples are irregularly spaced in time [4,5], and where samples are taken at unknown locations [6,7], among others. On the other hand, reconstructibility results have been established for multiple signal classes, from bandlimited signals [2], to signals in general shift-invariant subspaces [8], and signals of finite rate of innovation [9,10]. In short, classical sampling is well established and understood. Nonetheless, transitioning to a time encoding paradigm presents additional advantages.

On the one hand, time encoding can help us to better understand biology. Time encoding machines can be made to resemble biological neurons to different degrees. Here, we study perfect integrators that reset once a threshold is reached, but one can also investigate encoding and decoding using leaky integrate-and-fire neurons with refractory periods [11] or even Hodgkin Huxley neurons [12] for more biological resemblance. One can then hope that understanding time encoding can help to better understand the neural code. Moreover, and perhaps more practically, neural networks are often constructed using spiking neurons [13]. Then, understanding the basic components in spiking neural networks can help us understand their functioning and their constraints, as well as understand how to better take advantage of neuromorphic hardware [14].

On the other hand, time encoding can help us to improve man-made systems. In fact, time encoding can help us in designing higher-precision sampling hardware as high-precision clocks are more readily available than high-precision quantizers [1]. It can also help in reducing power consumption. It has been shown that single-channel time encoding has similar capabilities as traditional sampling: with time encoding, one can sample and reconstruct bandlimited signals [1,15,16] as well as signals with finite rate of innovation [17]. Here, we will show that time encoding also provides an advantage over classical sampling when it comes to multi-channel encoding. Indeed, we show that, in time encoding, reconstruction from multi-channel sampling with unknown initial conditions is no harder than reconstruction using single-channel sampling. This is not the case in classical sampling.

In this paper, we study multi-channel time encoding, where a bandlimited signal is input to  $M > 1$  time encoding machines that generate different outputs because of a shift in their integrator values. To make the analogy with neuroscience, it seems intuitive (at least from advances in machine learning), that multiple neurons can encode a signal better than one. Here, we would like to quantify this improvement when using TEMs which resemble neurons with perfect integrators.

Multi-channel encoding has been studied in the classical sampling setup by Papoulis who showed that a bandlimited

This work was in part supported by the Swiss National Science Foundation grant number 200021\_181978/1, “SESAM - Sensing and Sampling: Theory and Algorithms”.

Karen Adam, Adam Scholefield and Martin Vetterli are with the School of Computer and Communication Sciences, Ecole Polytechnique Fédérale de Lausanne (EPFL), CH-1015 Lausanne, Switzerland, email: first-name.lastname@epfl.ch.

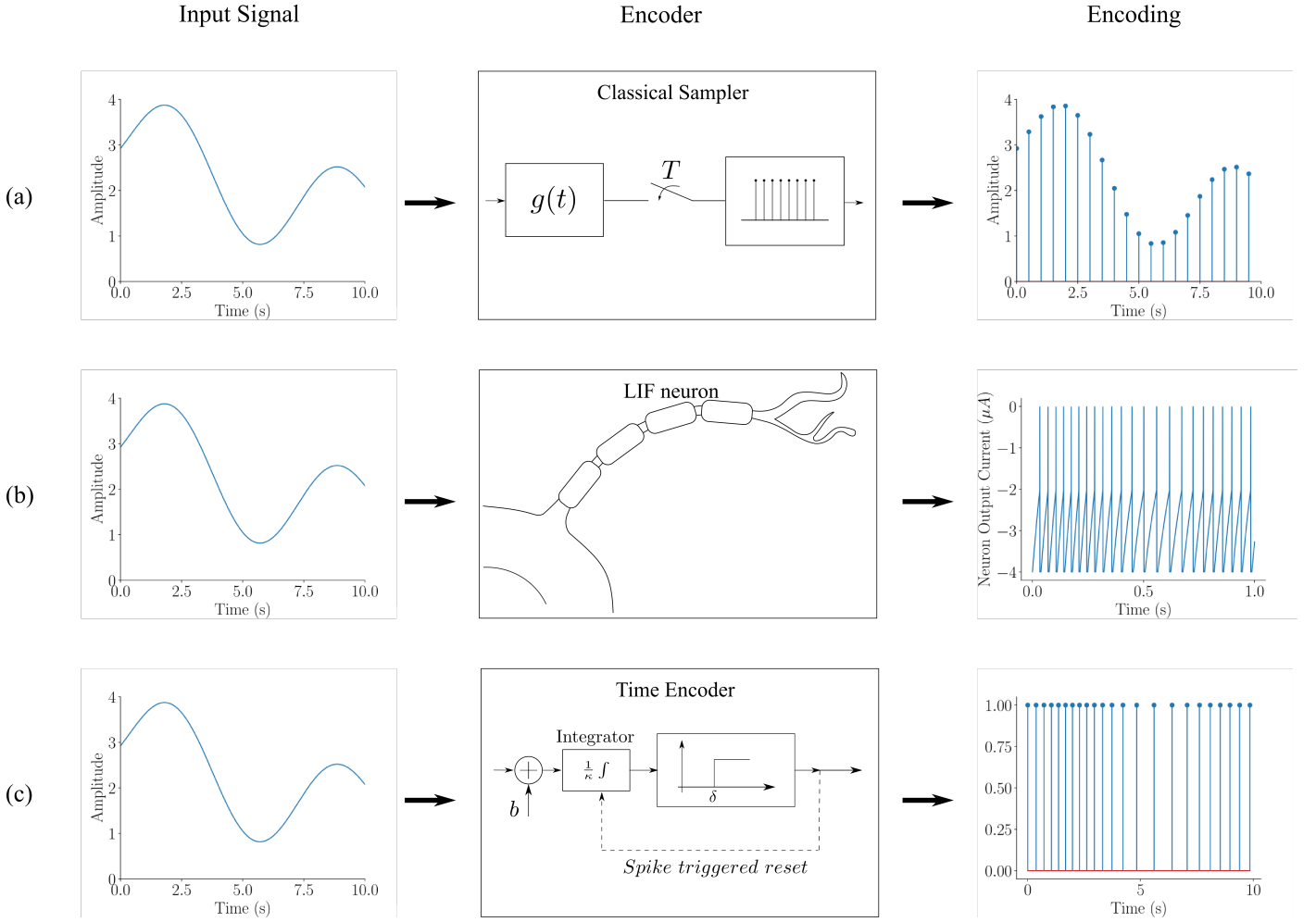


Fig. 1: Encoding of the same signal using different encoding modalities: **(a)** a classical sampler, **(b)** a leaky-integrate and fire (LIF) neuron, and **(c)** a time encoding machine. In **(a)** the signal is convolved with a kernel  $g(t)$ , commonly assumed to be a sinc function if the input signal is bandlimited for example, and then sampled every  $T$  seconds. The output is then a series of equally spaced (time, amplitude) pairs. In **(b)**, we assume that the signal is injected as a current into a spiking leaky-integrate-and-fire neuron following the model described in [18] and implemented using a spiking neural network simulator called Brian [19]. The recorded output is the outgoing current which exhibits a series of action potentials, or spikes. In **(c)**, the signal is input to a time encoding machine, as will be described in Section II, and the output is a series of signal-dependent trigger times. Notice how, in both **(b)** and **(c)**, the output spike streams are denser when the signal is stronger and sparser when the signal is weaker.

signal can be reconstructed from its samples from  $M$  channels using  $1/M$  the sampling rate [20]. Along similar lines, Lazar et al. considered multi-channel TEMs, where the channel is prefiltered with a linearly independent filter before time encoding [11,21]. To reconstruct, each channel is independently decoded reproducing that channel's post-filtered continuous-time signal and, finally, these are combined to reproduce the original signal.

In this paper, we suggest a setup without any prefiltering of the signal, where improved reconstruction relies on different time encoding machines having different outputs because of different and unknown configurations. We presented preliminary work on this topic in [22]. Here, we present a more intuitive algorithm, with an improvement on the maximum

bandwidth that can be perfectly reconstructed.

More precisely, we show that, if a bandlimited signal with bandwidth  $\Omega$  can be reconstructed using one TEM, then, using a Projection onto Convex Sets (POCS) algorithm, a bandlimited signal with bandwidth  $M\Omega$  can be reconstructed from  $M$  TEMs with the same parameters, as long as the machines are shifted with nonzero shifts. We also show that the reconstruction algorithm and conditions do not require the knowledge of the shifts, as long as these are nonzero. This is an important improvement over [22], where we only showed that this bound could be achieved if shifts between the machines were equally spaced, which is not easy to achieve in practice. The bound we propose here generalizes to all shift configurations.

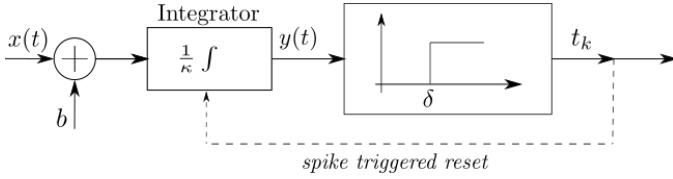


Fig. 2: Circuit of a time encoding machine with input  $x(t)$  and parameters  $\kappa$ ,  $\delta$  and  $b$ , where  $\kappa$  is the integrator constant,  $\delta$  is a threshold above which a spike is triggered and  $b$  is a positive bias added to the signal.

## II. SINGLE-CHANNEL TEM

### A. Time Encoding Definition

There are different variations of time encoding [1,11,23,24], but we consider the case where a time encoding machine (TEM) acts like an integrate-and-fire neuron with a perfect integrator and no refractory period<sup>1</sup>.

**Definition 1.** A *time encoding machine* (TEM) with parameters  $\kappa$ ,  $\delta$ , and  $b$  takes an input signal  $x(t)$ , adds to it a bias  $b$ , and integrates the result, scaled by  $1/\kappa$ , until a threshold  $\delta$  is reached. Once this threshold is reached, a time is recorded, the value of the integrator resets to  $-\delta$  and the mechanism restarts. We say that the machine spikes at the integrator reset and call the corresponding recorded time  $t_k$  a *spike time*.

Figure 2 depicts the circuit of a TEM and Fig. 3 provides an example of how an input generates its output.

Note how our definition of a sample has changed. In traditional sampling, a sample denoted a (time, amplitude) pair, whereas here, a sample denotes a spike time. We use the terminology “spike time”, to keep the analogy with integrate-and-fire neurons which produce responses by emitting action potentials. These action potentials have a fixed shape and amplitude<sup>2</sup>, so the relevant information in a neuron’s output lies in the *timing* of these action potentials, or spikes.

### B. Iterative Reconstruction of Bandlimited Signals

Results on signal reconstruction from the output of a TEM have been obtained for cases where the input is a  $c$ -bounded,  $2\Omega$ -bandlimited signal.

**Definition 2.** A signal is  $2\Omega$ -bandlimited and  $c$ -bounded if its Fourier transform is zero for  $|\omega| > \Omega$  and  $|x(t)| < c$  where  $c \in \mathbb{R}$ .

In [1], it is shown that such a signal can be perfectly reconstructed from the samples obtained from a TEM with parameters  $\kappa$ ,  $\delta$ , and  $b$  if,  $b > c$  and

$$\Omega < \frac{\pi(b-c)}{2\kappa\delta}. \quad (1)$$

<sup>1</sup>Note that this is slightly different from the definition provided in [1].

<sup>2</sup>There are two types of action potentials: the all-or-none action potential has a fixed amplitude, whereas the graded action potential can have a varying amplitude. The integrate-and-fire model assumes that action potentials are all-or-none, and not graded, although graded action potentials can also be found in biology.

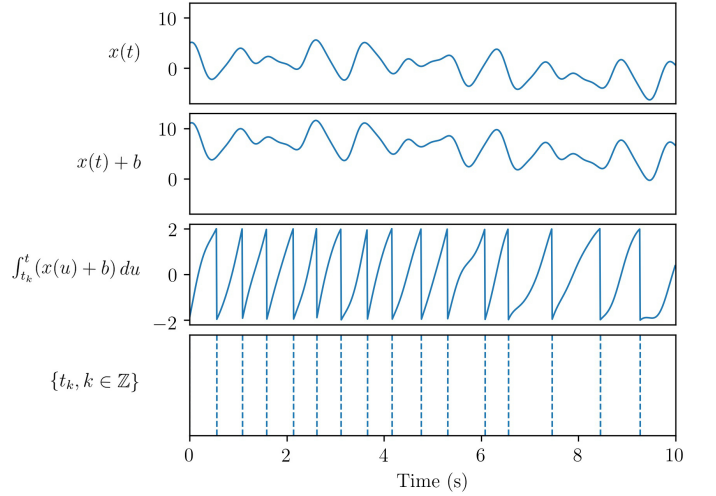


Fig. 3: Processing of a signal as it goes through the different stages of a time encoding machine. From top to bottom, we have: the input signal, the result of the bias addition, the result of the integration and the spike stream output.

The reconstruction algorithm uses the spike times  $t_k$  to compute integrals of the original signal. Indeed, if  $x(t)$  is our input signal and  $\{t_k, k \in \mathbb{Z}\}$  is the set of spike times recorded by our TEM, then we can compute

$$\int_{t_k}^{t_{k+1}} x(u) du = 2\kappa\delta - b(t_{k+1} - t_k), \quad (2)$$

where  $t_k$  and  $t_{k+1}$  are any two consecutive trigger times. Now, let  $\mathcal{A}$  be the following reconstruction operator:

$$\mathcal{A}x(t) = \sum_{k \in \mathbb{Z}} \int_{t_k}^{t_{k+1}} x(u) du g(t - s_k), \quad (3)$$

where  $s_k = (t_k + t_{k+1})/2$  and  $g(t) = \sin(\Omega t)/(\pi t)$ . One can then estimate  $x(t)$  iteratively by setting

$$x_0 = \mathcal{A}x, \quad (4)$$

$$x_{l+1} = x_l + \mathcal{A}(x - x_l). \quad (5)$$

To prove that the reconstruction algorithm converges if (1) is satisfied, one requires a bound on the separation between spike times: we recall that  $|x(t)| \leq c$ , which, when substituted into (2), yields

$$\begin{aligned} -c(t_{k+1} - t_k) &\leq 2\kappa\delta - b(t_{k+1} - t_k), \\ t_{k+1} - t_k &\leq \frac{2\kappa\delta}{b-c}. \end{aligned} \quad (6)$$

Then, one can use Bernstein and Wirtinger’s inequalities (Lemmas 8 and 9 of Appendix A) to prove convergence of the algorithm described in (3)-(5). In short, it is shown in [1] that the given algorithm can perfectly reconstruct a  $c$ -bounded,  $2\Omega$ -bandlimited signal from the samples of a TEM with parameters  $\kappa$ ,  $\delta$  and  $b$ , given that  $c < b$  and  $\Omega$  satisfies (1).

Notice that this result imposes a Nyquist-like constraint on the bandwidth: (1) requires a bandwidth which is inversely

proportional to the separation between spike times. Reconstruction of the original signal is then very similar to the reconstruction of a bandlimited signal sampled with irregularly spaced amplitude samples [4].

### C. Matrix Formulation of Bandlimited Signal Reconstruction

In [1], Lazar et al. also obtain a closed-form matrix formulation for the above recursive algorithm. First, let  $\mathcal{G}$  be the operator defined as

$$\mathcal{G}y = \sum_{k \in \mathbb{Z}} y_k g(t - s_k),$$

where  $s_k = (t_k + t_{k+1})/2$  and  $g(t) = \sin(\Omega t)/(\pi t)$  as before. In addition, define

$$\mathbf{q} = \left[ \int_{t_k}^{t_{k+1}} x(u) du \right]_{k \in \mathbb{Z}},$$

and

$$\mathbf{H} = [H_{\ell k}]_{\ell, k \in \mathbb{Z}} = \left[ \int_{t_\ell}^{t_{\ell+1}} g(u - s_k) du \right]_{\ell, k \in \mathbb{Z}}.$$

Then, one can write  $x(t) = \mathcal{G}\mathbf{H}^+ \mathbf{q}$  where  $\mathbf{H}^+$  is the pseudoinverse of  $\mathbf{H}$ . We refer the reader to [1] for a proof.

We have covered the main results established in [1] and now wish to reformulate the reconstruction algorithm from the perspective of projections onto convex sets. We will later use this perspective to present a solution for multi-channel sampling and reconstruction.

### III. SINGLE-CHANNEL TEM: A POCS PERSPECTIVE

We wish to reach a more intuitive interpretation of the recursive algorithm presented above, to adapt it to new, potentially more complex scenarios. Let  $\mathcal{A}_1$  be our time encoding machine, and let  $\mathcal{A}$  be defined as in (3); we can rewrite it as follows:

$$\begin{aligned} \mathcal{A}x(t) &= \left( \sum_{k \in \mathbb{Z}} \int_{t_k}^{t_{k+1}} x(u) du \delta(t - s_k) \right) * g(t), \\ &= \mathcal{B}x(t) * g(t), \end{aligned} \quad (7)$$

where  $\mathcal{B}$  is defined as

$$\mathcal{B}x(t) = \sum_{k \in \mathbb{Z}} \int_{t_k}^{t_{k+1}} x(u) du \delta(t - s_k). \quad (8)$$

By recursion, we can show that  $x_\ell(t)$ , as defined in (4) and (5), is bandlimited with bandwidth  $2\Omega$  at every iteration  $\ell$ . Therefore,

$$\begin{aligned} x_{\ell+1} &= x_\ell * g + \mathcal{B}(x - x_\ell) * g, \\ &= (x_\ell + \mathcal{B}(x - x_\ell)) * g. \end{aligned}$$

Recall that  $g(t) = \sin(\Omega t)/(\pi t)$ .

We can thus divide the computation of  $x_{l+1}$  into two steps:

$$x_{\ell+1} = \mathcal{P}_\Omega(\mathcal{P}_{\mathcal{A}_1}(x_\ell)), \quad (9)$$

where

$$\mathcal{P}_{\mathcal{A}_1}y(t) = y(t) + \mathcal{B}(x(t) - y(t)), \quad (10)$$

and

$$\mathcal{P}_\Omega y(t) = y(t) * g(t). \quad (11)$$

Letting  $\mathcal{C}_\Omega$  be the space of  $2\Omega$ -bandlimited functions, we have the following two lemmas.

**Lemma 1.**  $\mathcal{P}_\Omega$  is a projection operator onto  $\mathcal{C}_\Omega$ .

*Proof:* See Appendix B. ■

**Lemma 2.**  $\mathcal{C}_\Omega$  is convex.

*Proof:* See Appendix B ■

As for  $\mathcal{P}_{\mathcal{A}_1}$ , we can substitute (8) into (10), yielding

$$\mathcal{P}_{\mathcal{A}_1}y(t) = y(t) + \sum_{k \in \mathbb{Z}} \int_{t_k}^{t_{k+1}} [x(u) - y(u)] du \delta(t - s_k). \quad (12)$$

We thus see that the operator depends on the spike times  $t_k$  emitted by a TEM with input  $x(t)$ . In words, this operator adds a Dirac to  $y(t)$  at the midpoint  $s_k$  of each interval  $[t_k, t_{k+1}]$ . The amplitude of these Diracs is such that  $\int_{t_k}^{t_{k+1}} \mathcal{P}_{\mathcal{A}_1}(y(u)) du = \int_{t_k}^{t_{k+1}} x(u) du$ ,  $\forall k$ ; i.e., the projected signal agrees with the measurements.

Now, let  $\mathcal{C}_{\mathcal{A}_1}$  be the space of functions  $y(t)$  satisfying  $\int_{t_k}^{t_{k+1}} y(u) du = \int_{t_k}^{t_{k+1}} x(u) du$ ,  $\forall k \in \mathbb{Z}$ .

**Lemma 3.**  $\mathcal{P}_{\mathcal{A}_1}$  is a projection operator onto  $\mathcal{C}_{\mathcal{A}_1}$ .

*Proof:* See Appendix B. ■

**Lemma 4.**  $\mathcal{C}_{\mathcal{A}_1}$  is convex.

*Proof:* See Appendix B ■

Since both  $\mathcal{P}_{\mathcal{A}_1}$  and  $\mathcal{P}_\Omega$  are projection operators onto  $\mathcal{C}_{\mathcal{A}_1}$  and  $\mathcal{C}_\Omega$  respectively, the entire iterative reconstruction algorithm then consists of alternately projecting onto two sets, each being convex.

We have thus shown that our reconstruction algorithm for single-channel time encoding consists of an alternating projection onto convex sets (POCS) algorithm [25]–[27].

**Definition 3.** The *projection onto convex sets (POCS) method* assumes that the element we are looking for lies in the intersection of  $N$  known convex sets,  $\mathcal{C}_1, \mathcal{C}_2, \dots, \mathcal{C}_N$ , and proceeds by alternately projecting on each of them using operators  $\mathcal{P}_1, \mathcal{P}_2, \dots, \mathcal{P}_N$ .

The POCS algorithm is known to converge to a fixed point which lies in the intersection of the sets at hand  $\bigcap_{i=1}^N \mathcal{C}_i$  [26]. Thus, if the intersection of the sets consists of a single element, then the algorithm converges to the *correct* solution.

Adopting a POCS interpretation of our algorithm allows us to directly deduce that the algorithm converges to a fixed point in the intersection of the sets of  $2\Omega$ -bandlimited functions, and functions which generate the spike times of the TEM. The fact that the fixed point is unique and that it is indeed the original signal is guaranteed by the proof provided in [1], which relies on the maximal separation between spike times, and Bernstein's and Wirtinger's inequalities. Uniqueness can also be proven in a similar fashion to our proof in Section IV-C.

#### IV. M-CHANNEL TEM

##### A. M-Channel TEM Definition

First let us define an  $M$ -channel time encoding machine.

**Definition 4.** An  $M$ -channel time encoding machine consists of  $M$  single-channel TEMs  $A_1, A_2, \dots, A_M$ , with parameters  $\kappa, \delta$  and  $b$ , and which spike in this order  $A_1, A_2, \dots, A_M$ , i.e.

$$t_{k-1}^{(i+1)} < t_k^{(i)} < t_k^{(i+1)} \quad \forall k, \forall i = 1 \dots M-1, \quad (13)$$

$$t_k^{(1)} < t_k^{(M)} < t_{k+1}^{(1)} \quad \forall k, \quad (14)$$

where  $\{t_k^{(i)}, k \in \mathbb{Z}\}$  is the set of spike times emitted by TEM  $A_i$ .

Equations (13) and (14) force a strict order of the spike times on the  $M$  machines, i.e. all machines have different outputs. At first glance, it seems strange that TEMs with the same parameters would have different outputs, but this occurs when there are nonzero integrator shifts between the channels.

**Definition 5.**  $M$  TEMs have *integrator shifts*  $\alpha_1, \alpha_2, \dots, \alpha_M$  if, for the same input  $x(t)$ , and for any time  $t$ , the outputs of the integrators  $y_1(t), y_2(t), \dots, y_M(t)$  satisfy

$$y_{i+1}(t) = (y_i(t) + \alpha_i) \mod 2\delta, \quad i = 1 \dots M-1 \quad (15)$$

$$y_1(t) = (y_M(t) + \alpha_M) \mod 2\delta. \quad (16)$$

Here,  $\sum_i \alpha_i = 2\delta$ .

Figure 4 shows an example of 2-channel time encoding. We pass an input signal through the two single-channel TEMs (with nonzero integrator shifts) and record the output of each integrator. Notice how the integrator values are always shifted by the same amount (modulo  $2\delta$ ). In contrast, if the integrator shifts between the two channels were zero, the output of both integrators would match at all time points. However, in the example presented, the integrators are shifted by a nonzero amount. Therefore, as the spike times are generated at the integrator reset, the TEMs are guaranteed to spike at different times.

Given the ordering enforced by the nonzero integrator shifts, as made explicit in (13) and (14), the spike times of all TEMs are distinct. In other words, there exists no combination of  $k, \ell, i$  and  $j$  such that

So far, we have assumed that our signals have infinite support, and that our TEM samples the signal for infinite time. In practice, however, a TEM would start recording a signal at a certain time  $t_{start}$  and stop recording at  $t_{end}$ . In these scenarios, integrator shifts can be well defined and implemented.

Indeed, these integrator shifts will result from different initial conditions on the integrators of the TEMs at  $t_{start}$ . For example, assume TEMs  $A_1$  and  $A_2$  start integrating at the same time  $t_{start}$  with initial values  $y_1(t_{start})$  and  $y_2(t_{start})$ , respectively. Then TEM  $A_2$  will always lead TEM  $A_1$  by  $\alpha_1 = y_2(t_{start}) - y_1(t_{start})$ .

More practically, an integrator is represented in circuitry by an operational amplifier coupled with a resistor and capacitor, as seen in Fig. 5. This capacitor can be charged with a

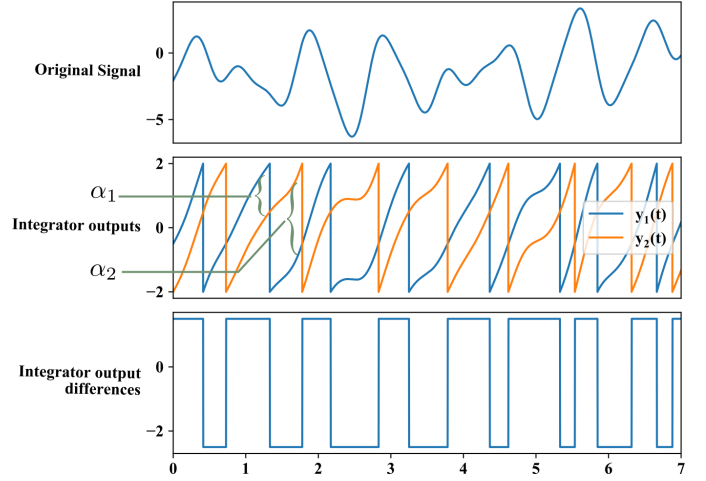


Fig. 4: Output of the integrators of two TEMs with nonzero shifts. We assume both TEMs have a threshold  $\delta = 2$  and that TEM  $A_2$  is leading TEM  $A_1$  by  $\alpha_1 = 0.75$ . This means  $y_2(t) = y_1(t) + \alpha_1 \mod 2\delta, \forall t$ . We plot, from top to bottom: The original signal input to the machines, the output of the integrator of each machine ( $y_i(t)$  corresponding to the output of the integrator of TEM  $A_i$ ), and the difference between the outputs of the two machines.

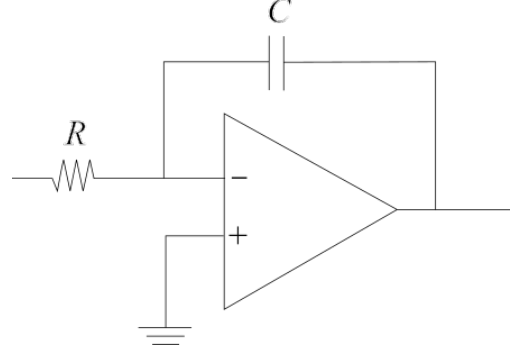


Fig. 5: The circuit of an integrator comprises of an operational amplifier, a resistor  $R$  and a capacitor  $C$  in this configuration. The circuit does not provide a perfect integrator as we require in our model but it serves a good approximation of it and allows the implementation of our setup in hardware. An analysis of time encoding using leaky integrators such as this one is presented in [21].

certain voltage before the input is fed into the circuit. This initial charge of the capacitor can practically implement the initial value of the integrator. Therefore, having different initial charges on the capacitors of each machine would lead to nonzero integrator shifts.

However, we recall that our setup assumes a perfect integrator and infinite time support. The initial conditions formulation in this section serves as a more intuitive explanation of how integrator shifts arise, and as a practical explanation of where these shifts come from, in hardware.

### B. Convergence of $M$ -Channel Reconstruction using POCS

We use the POCS formulation to devise a reconstruction algorithm for multi-channel time encoding, thus extending the result found in [1] to the case where  $x(t)$  is sampled using multiple independent time encoding machines.

In [22], we presented an algorithm that could reconstruct  $2\Omega$ -bandlimited signals from an  $M$ -channel TEM if

$$\Omega < \frac{\pi(b-c)}{2\kappa\bar{\alpha}}. \quad (17)$$

Here,  $\bar{\alpha} = \max_{i=1 \dots M} \alpha_i$  depends on the shifts between the machines. In this scenario, we reached the maximal possible bandwidth if the machine integrators were spaced in such a way that  $\bar{\alpha} = \alpha_i = 2\delta/M$ ,  $\forall i = 1 \dots M$ . Then, the bandwidth could improve by a factor of  $M$  compared to the single channel case.

In this paper, we want to show that, in the  $M$ -channel case, the improvement on  $\Omega$  is always  $M$ -fold, regardless of the spacing between the machines' integrators, as long as this spacing is nonzero.

To do this, we will design an algorithm that reconstructs an input from its  $M$ -channel spiking output and provide conditions for its convergence. We use as inspiration the POCS interpretation of the single-channel reconstruction algorithm.

The POCS method can guarantee convergence onto a fixed point by alternately projecting onto convex sets. The averaged projection method works similarly.

**Definition 6.** The *averaged projections method* assumes that we have  $N$  convex sets  $\mathcal{C}_1, \dots, \mathcal{C}_N$  with corresponding projection operators  $\mathcal{P}_1, \dots, \mathcal{P}_N$  and that we compute an estimate of  $x$  at iteration  $\ell + 1$  by taking

$$x_{\ell+1} = \frac{1}{N} \sum_{i=1}^N \mathcal{P}_i(x_\ell). \quad (18)$$

This algorithm can be reduced into an alternating projection algorithm and therefore also converges to a fixed point in the intersection of the sets.

We design an algorithm for reconstructing  $2\Omega$ -bandlimited signals from the encoding of more than one TEM. The algorithm will converge to a fixed point in the set of solutions that can produce the different time encodings. We will later find conditions on  $\Omega$  that are sufficient for this set of solutions to consist of a single element, so that our algorithm converges to the unique and desired solution. First, let us explain the algorithm.

Let  $A_1, A_2, \dots, A_M$  be our  $M$  time encoding machines, and let  $\{t_k^{(i)}, k \in \mathbb{Z}\}$  be the spike times emitted by machine  $i$ ,  $i = 1 \dots M$ , when the input is  $x(t)$ —a  $2\Omega$ -bandlimited signal such that  $|x(t)| < c$ , for some  $c \in \mathbb{R}$ .

Then, let  $\mathcal{A}_i$  be the reconstruction operator associated with machine  $i$ , so that

$$\mathcal{A}_i x(t) = \sum_{k \in \mathbb{Z}} \int_{t_k^{(i)}}^{t_{k+1}^{(i)}} x(u) du \ g\left(t - s_k^{(i)}\right). \quad (19)$$

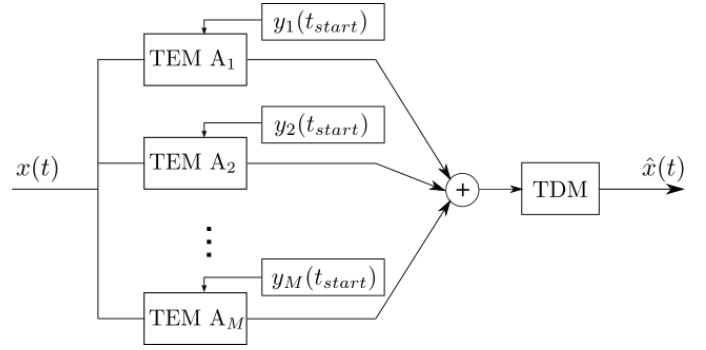


Fig. 6: Multi-channel time encoding and decoding pipeline. In Practice, the TEMs are initialized with some initial value of their integrators  $y_i(t_{start})$  and the integrator shift between two machines  $A_i$  and  $A_{i+1}$  is  $\alpha_i = y_{i+1}(t_{start}) - y_i(t_{start}) \bmod 2\delta$ , for  $1 < i < M$  (the shift between machines  $A_M$  and  $A_1$  is  $\alpha_M = y_1(t_{start}) - y_M(t_{start}) \bmod 2\delta$ ). The output streams of the different machines can be combined into one before being fed into a single decoding machine because of the perfect ordering of the spikes provided in (13) and (14).

Then, define a new reconstruction operator

$$\mathcal{A}_{1 \dots M} = \frac{1}{M} \sum_{i=1}^M \mathcal{A}_i \quad (20)$$

and recursively estimate  $x(t)$  by setting

$$x_0 = \mathcal{A}_{1 \dots M} x, \quad (21)$$

$$x_{\ell+1} = x_\ell + \mathcal{A}_{1 \dots M}(x - x_\ell). \quad (22)$$

This algorithm is equivalent to taking alternating projections on the set  $\mathcal{C}_\Omega$  and the sets  $\mathcal{C}_{A_i}$ , where  $\mathcal{C}_\Omega$  denotes the set of  $2\Omega$ -bandlimited functions and each  $\mathcal{C}_{A_i}$  denotes the set of functions that could have potentially generated the spike times of machine  $A_i$ . All of these sets are convex by Lemmas 2 and 4.

The algorithm then converges to a solution that is  $2\Omega$ -bandlimited and that can generate the spike times  $\{t_k^{(i)}, k \in \mathbb{Z}\}$ ,  $\forall i = 1 \dots M$ . Note that this algorithm does not require knowing the shifts  $\alpha_i$  between the integrators of the machines, it only requires knowing the parameters  $\kappa$ ,  $\delta$  and  $b$  of the machines.

So far, we have only shown that the algorithm converges to a fixed point that satisfies  $2\Omega$ -bandlimitedness and is consistent with the spike times generated by all machines  $A_i$ ,  $i = 1 \dots M$ .

In the next section, we show that this solution is unique (and is thus the originally sampled signal), if the signal is  $2\Omega$ -bandlimited where

$$\Omega < \frac{M\pi(b-c)}{2\kappa\delta}. \quad (23)$$

We recall that  $M$  is the number of machines,  $\kappa$ ,  $\delta$  and  $b$  are the parameters of the individual machines and  $c$  is the bound on the input signal  $x(t)$ , i.e  $|x(t)| < c$ . Before we proceed to prove uniqueness, we show, in Fig. 7, a reconstruction example



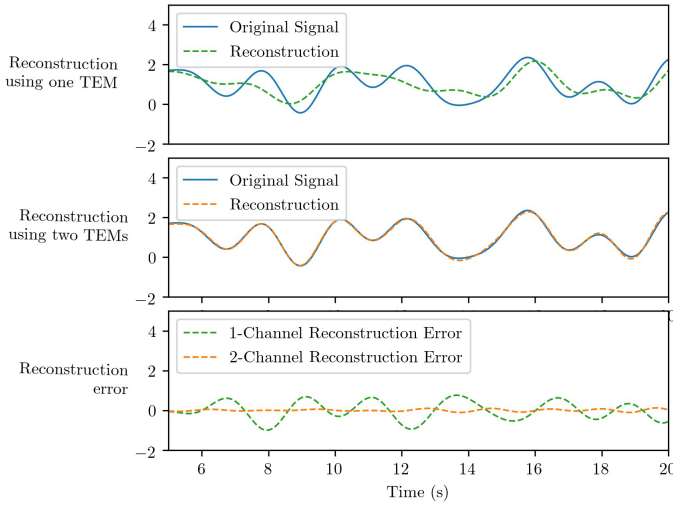


Fig. 7: (Top) Reconstruction of a signal from its time encoding, using one channel. (Middle) Reconstruction of the same signal from its time encoding using two channels with integrators shifted by an unknown value. (Bottom) Reconstruction error when using outputs of 1-channel TEM and 2-channel TEM.

demonstrating that the algorithm we suggested for the  $M$ -channel case can reconstruct a wider range of signals than is possible in the single channel case.

### C. Uniqueness of $M$ -Channel Reconstruction using POCS

We have presented an algorithm which converges to a fixed point in the intersection of the  $\mathcal{C}_{A_i}$ 's with  $\mathcal{C}_\Omega$ ; we now wish to pinpoint sufficient conditions for this intersection to be unique.

Assume the input signal,  $x(t)$ , is a  $2\Omega$ -bandlimited signal in  $L^1(\mathbb{R})^3$ . We wish to find an estimate of it, which we denote  $\hat{x}(t)$ , using the output spike times of  $M$  time encoding machines. By applying the algorithm we described in (20)-(22),  $\hat{x}(t) = \lim_{\ell \rightarrow \infty} x_\ell(t)$  will be a fixed point in the intersection of the sets  $\mathcal{C}_{A_i}$  with  $\mathcal{C}_\Omega$ , so  $\hat{x}(t)$  will lie in every one of the  $\mathcal{C}_{A_i}$ 's. This means that for every  $i = 1 \dots M$ ,

$$\int_{t_k^{(i)}}^{t_{k+1}^{(i)}} \hat{x}(u) du = \int_{t_k^{(i)}}^{t_{k+1}^{(i)}} x(u) du, \quad \forall k \in \mathbb{Z}. \quad (24)$$

Let us denote  $X(t) = \int_{-\infty}^t x(u) du$  and  $\hat{X}(t) = \int_{-\infty}^t \hat{x}(u) du$ . Then it follows that  $X(t_{k+1}^{(i)}) - X(t_k^{(i)}) = \hat{X}(t_{k+1}^{(i)}) - \hat{X}(t_k^{(i)})$ ,  $\forall k \in \mathbb{Z}$ .

**Lemma 5.**  $X(t_k^{(i)}) = \hat{X}(t_k^{(i)})$ ,  $\forall k \in \mathbb{Z}$ ,  $\forall i = 1 \dots M$ .

<sup>3</sup>A signal  $x(t)$  is in  $L^1(\mathbb{R})$  if  $\|x(t)\|_1 = \int_{\mathbb{R}} |x(u)| du < \infty$ .

*Proof:*

$$\begin{aligned} X(t_k^{(i)}) &\stackrel{(a)}{=} \int_{-\infty}^{t_k^{(i)}} x(u) du \\ &\stackrel{(b)}{=} \lim_{k \rightarrow \infty} \sum_{\ell=-\infty}^{k-1} (X(t_{\ell+1}^{(i)}) - X(t_\ell^{(i)})) \\ &\stackrel{(c)}{=} \lim_{k \rightarrow \infty} \sum_{\ell=-\infty}^{k-1} (\hat{X}(t_{\ell+1}^{(i)}) - \hat{X}(t_\ell^{(i)})) \\ &\stackrel{(d)}{=} \int_{-\infty}^{t_k^{(i)}} \hat{x}(u) du \\ &\stackrel{(e)}{=} \hat{X}(t_k^{(i)}), \quad \forall k \in \mathbb{Z}, \end{aligned}$$

where equalities (a) and (e) follow from the definitions of  $X(t)$  and  $\hat{X}(t)$ , respectively, (b) and (d) follow from  $x(t)$  and  $\hat{x}(t)$  being in  $L^1(\mathbb{R})$ , and (c) follows from the fact that  $X(t_{k+1}^{(i)}) - X(t_k^{(i)}) = \hat{X}(t_{k+1}^{(i)}) - \hat{X}(t_k^{(i)})$ ,  $\forall k \in \mathbb{Z}$ . So  $X(t)$  and  $\hat{X}(t)$  match at all  $t_k^{(i)}$ ,  $k \in \mathbb{Z}$ ,  $i = 1 \dots M$ . ■

**Lemma 6.** The integrals  $X(t)$  and  $\hat{X}(t)$  are both  $2\Omega$ -bandlimited.

*Proof:* The original signals  $x(t)$  and  $\hat{x}(t)$  are both  $2\Omega$ -bandlimited, and, since they are also in  $L^1(\mathbb{R})$ , they have zero mean. Taking the integrals of these signals corresponds to a division by  $j\omega$  in the frequency domain, where  $\omega$  denotes the frequency, so the frequency content of  $X(t)$  and  $\hat{X}(t)$  remains concentrated in  $[-\Omega, \Omega]$ . ■

Therefore,  $X(t)$  and  $\hat{X}(t)$  are two  $2\Omega$ -bandlimited functions which coincide at time points  $t_k^{(i)}$ ,  $\forall k \in \mathbb{Z}$ ,  $\forall i = 1 \dots M$ . In other words, if both  $X(t)$  and  $\hat{X}(t)$  are sampled at the  $t_k^{(i)}$ 's, their samples would have the same values.

Let us combine and order all spike times from the machines into one set  $\{\tilde{t}_k, k \in \mathbb{Z}\}$ . To show that these samples are sufficient to ensure that  $X(t)$  and  $\hat{X}(t)$  match, we use a result from Jaffard. In [5], he proved that a sampling sequence  $\{t_k, k \in \mathbb{Z}\}$  generates a frame for  $\mathcal{C}_\Omega$  if and only if  $\{t_k, k \in \mathbb{Z}\}$  is relatively separated and

$$\liminf_{r \rightarrow \infty} \frac{n(r)}{r} > \frac{\Omega}{\pi}, \quad (25)$$

where  $n(r)$  is the number of samples in an interval of length  $r$ .

This finding provides conditions for irregular (time, amplitude) samples to completely characterize a bandlimited signal: the sample set has to be relatively separated, and the average sampling rate needs to be higher than the Nyquist rate.

Requiring that the sampling set be relatively separated is a technical condition which ensures a minimum separation between sample times. In Appendix B, we formally define it (Definition 7) and show that the sampling set  $\{\tilde{t}_k, k \in \mathbb{Z}\}$  is relatively separated (Lemma 10). On the other hand, to help us prove that the Nyquist-like condition is satisfied, the following lemma provides us with a lower bound on the average sampling rate of our spike times  $\{\tilde{t}_k, k \in \mathbb{Z}\}$ .

**Lemma 7.** *The sampling set  $\{\tilde{t}_k, k \in \mathbb{Z}\}$  has an average sampling rate which is at least  $M(b-c)/(2\kappa\delta)$ .*

*Proof:* Spike times have a maximal separation between them defined by (6). According to this bound, every machine produces a sampling set  $\{t_k^{(i)}, k \in \mathbb{Z}\}$  where two spike times have a separation of at most  $2\kappa\delta/(b-c)$ . Therefore, the sampling rate  $n(r)/r$  is at least  $(b-c)/2\kappa\delta$ , for any  $r \in \mathbb{R}$ . Therefore, the average sampling rate of a machine  $\liminf_{r \rightarrow \infty} n(r)/r$  is at least  $(b-c)/2\kappa\delta$ . Since all machines fire at distinct time points (because the shifts between them are nonzero), together, they have an average sampling rate which is at least  $M(b-c)/2\kappa\delta$ . ■

It follows that the samples emitted by the TEMs are sufficient to determine uniqueness for a  $2\Omega$ -bandlimited signal, provided that  $\Omega$  satisfies (23).

Hence, a signal  $X(t)$  which is  $2\Omega$ -bandlimited, with  $\Omega$  satisfying (23), is uniquely defined by the samples provided by a  $M$ -channel TEM with parameters  $\kappa, \delta$  and  $b$  and input  $x(t)$ , such that  $|x(t)| \leq c < b$  and  $x(t) \in L^1(\mathbb{R})$ . Therefore,  $X(t)$  and its estimate  $\hat{X}(t)$  match exactly, and as  $x(t)$  and  $\hat{x}(t)$  are their respective derivatives, they are also completely characterized by the samples and match exactly. So our reconstruction using this multi-channel time decoding algorithm is perfect in the noiseless case.

Our findings are summarized into the following theorem:

**Theorem 1.** *Assume  $x(t)$  is a  $2\Omega$ -bandlimited signal in  $L^1(\mathbb{R})$  that is bounded such that  $|x(t)| \leq c$ . If  $x(t)$  is passed through  $M$  TEMs with parameters  $\kappa, \delta$  and  $b$ , such that  $b > c$ , the shifts  $\alpha_i, i = 1 \dots M$  between the TEMs are nonzero and*

$$\Omega < \frac{M\pi(b-c)}{2\kappa\delta},$$

*then if one estimates  $x_\ell(t)$  recursively by applying (19)-(22),*

$$\lim_{\ell \rightarrow \infty} x_\ell(t) = x(t). \quad (26)$$

We have thus shown that using  $M$  time encoding machines to encode a  $2\Omega$ -bandlimited signal  $x(t)$  allows a bandwidth  $\Omega$  which is  $M$  times larger than in the single channel case, no matter how the shifts between the machines are configured, as long as they are all nonzero. As already stated, we had shown in [22] that the bandwidth could become  $M$  times larger, but only if the machines were configured in such a way that their integrators had equally spaced values. In other words, if we denote  $y_i(t)$  to be the value of the integrator of machine  $i$ , then we required,  $\forall i = 1 \dots M-1$ ,

$$\alpha_i = y_{i+1}(t) - y_i(t) = 2\delta/M. \quad (27)$$

Configuring the integrator shifts between two machines is not easy (somewhat like synchronizing the clocks of different channels in classical sampling). Therefore, achieving maximal information gain becomes a harder feat. Here, we have shown that the bandwidth improvement by a factor of  $M$  is actually independent of the  $\alpha_i$ 's, as long as these are nonzero, and that the reconstruction algorithm does not require the knowledge of the  $\alpha_i$ 's.

The strength of this algorithm lies in its simplicity. We have  $M$  TEMs with integrators that are shifted with respect to each other by some shifts  $\alpha_i$ , and if the set of  $\alpha_i$ 's changes, the spike outputs of the machines change. However, this algorithm does not require knowledge of the shifts, it only operates on the spike times generated by the machine. Moreover, labelling of spike times according to the machine they come from is not necessary. TEMs are shifted with respect to each other by  $\alpha_i$ , so the order of spiking of the machines is fixed: we will always have spikes coming from TEM  $A_1, A_2, \dots, A_M, A_1, A_2, \dots$ . Therefore, the algorithm operates on a model as depicted in Fig. 6, and is still able to disentangle spike streams.

#### D. Closed Form Solution

The iterative algorithm that we have described can be reformulated to obtain a closed form solution for the problem.

First, let  $\{\tilde{t}_k, k \in \mathbb{Z}\}$  denote the set of combined and ordered spike times from all machines  $A_1, \dots, A_M$ . Now define

$$\tilde{\mathcal{G}}y = \sum_{k \in \mathbb{Z}} y_k g(t - \tilde{s}_k), \quad (28)$$

where  $\tilde{s}_k = (\tilde{t}_k + \tilde{t}_{k+M})/2$ .

Also define

$$\tilde{\mathbf{q}} = \left[ \int_{\tilde{t}_k}^{\tilde{t}_{k+M}} x(u) du \right]_{k \in \mathbb{Z}},$$

and

$$\tilde{\mathbf{H}} = [\tilde{H}_{\ell k}]_{\ell, k \in \mathbb{Z}} = \left[ \int_{\tilde{t}_\ell}^{\tilde{t}_{\ell+M}} g(u - \tilde{s}_k) du \right]_{\ell, k \in \mathbb{Z}}.$$

Then, one can show by induction that  $x_\ell$ , as defined in (20) - (22), can be expressed as

$$x_\ell = \tilde{\mathcal{G}} \sum_{k=0}^{\ell} (\mathbf{I} - \tilde{\mathbf{H}})^k \tilde{\mathbf{q}}. \quad (29)$$

Now we note that  $\lim_{\ell \rightarrow \infty} \sum_{k=0}^{\ell} (\mathbf{I} - \tilde{\mathbf{H}})^k = \tilde{\mathbf{H}}^+$ , where  $+$  denotes a pseudo-inverse. Therefore, a closed form solution for reconstructing  $x(t)$  under the same conditions as the ones posed in Theorem 1 is

$$\hat{x}(t) = \tilde{\mathcal{G}} \tilde{\mathbf{H}}^+ \tilde{\mathbf{q}}. \quad (30)$$

## V. SIMULATIONS

### A. Result Validation

We use the closed form solution of our reconstruction algorithm to run simulations that validate Theorem 1. In Fig. 8, we randomly generate one hundred  $2\Omega$ -bandlimited signals, for each value of  $\Omega = \pi, 2\pi, \dots, 20\pi$ . We provide the reconstruction error when using  $M = 1 \dots 10$  channels with the same parameters  $\kappa, \delta$  and  $b$  to sample and reconstruct the signals. The channels are constructed with equally spaced shifts, i.e. for an  $M$ -channel TEM, the integrator shifts are  $\alpha_i = 2\delta/M, \forall i = 1 \dots M$ . Note how reconstruction is



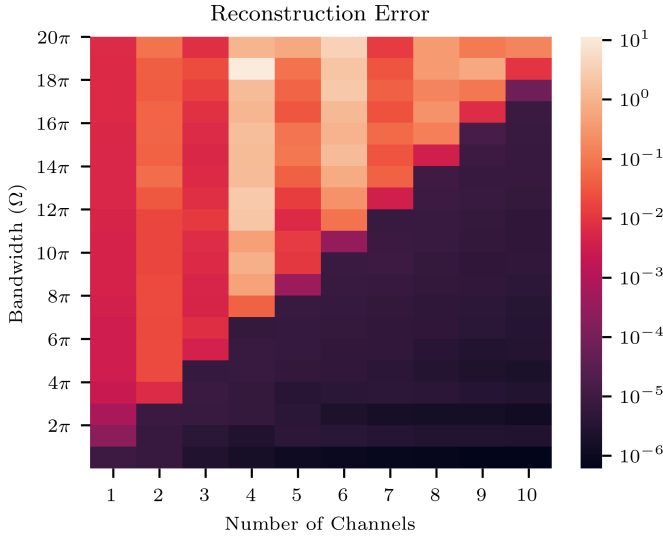


Fig. 8: Error of time encoding reconstruction when  $M = 1 \dots 10$  channels with equally-shifted integrators encode a signal as its bandwidth varies. The mean-squared error is averaged over one hundred trials and plotted as a function of the bandwidth and the number of samples.

successful for a wider bandwidth as the number of machines increases, and how the bound on the bandwidth increases linearly with the number of machines used. Note that all signals are normalized to have a power of 1 so that the reconstruction error is a comparable and meaningful metric.

To show that this  $M$ -fold improvement on the bound for the bandwidth is independent of the value of the shift, we evaluate the reconstruction error when signals are sampled using 2-channel TEMs with different values for the shift. In Fig. 9, we again simulate one hundred  $2\Omega$ -bandlimited signals where  $\Omega$  now varies between  $\pi/4$  and  $15\pi$ , and plot the averaged reconstruction error for 2-channel decoding, as well as the averaged reconstruction error for single-channel decoding. Notice how the reconstruction is successful for wider ranges of the bandwidth in the 2-channel case, compared to the single-channel case, and how different values of the integrator shifts between the two channels do not affect this region of success.

### B. Problem III-Conditioning for Small Shifts

We have shown that, in theory, the condition we placed in (23) is sufficient for the reconstruction algorithm to converge no matter the shifts between the integrators of different machines. Moreover, Fig. 9 verified this result for a few values of the integrator shifts. Intuitively, however, the problem should become more ill-posed as the shifts approach zero.

To investigate this, we evaluate the performance of two-channel time encoding and decoding as the shifts between the channels approach zero. We randomly generate one hundred  $2\Omega$ -bandlimited signals, where  $\Omega$  varies between  $\pi/4$  and  $16\pi$ . These signals are then encoded and decoded using two-channel TEMs with fixed parameters  $\kappa$ ,  $\delta$  and  $b$  and with varying shift

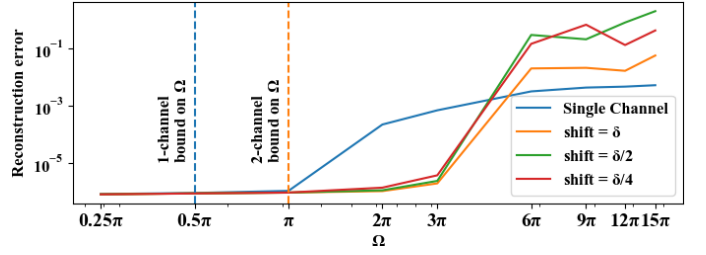


Fig. 9: Error of time encoding reconstruction, when using a single channel (blue), and when using 2 channels with different spacing configurations (orange, green, red). The mean-squared error is averaged over two hundred trials and plotted as a function of the bandwidth. When we denote a shift to have value  $\alpha$ , TEM  $A_2$  has its integrator  $\alpha$  ahead of TEM  $A_1$  (modulo  $2\delta$ ) and consequently, TEM  $A_1$  has its integrator  $2\delta - \alpha$  ahead of TEM  $A_2$  (modulo  $2\delta$ ). The closer the shift is to  $\delta$ , the more equally spaced the samples are expected to be.

$\alpha$ . We then estimate the reconstruction success by computing the reconstruction error.

Figure 10 is essentially a two dimensional version of the plot in Fig. 9 which investigates smaller shifts. As the integrator shift approaches zero, the outputs of the two channels of the TEM start to resemble each other more and more, so our two-channel encoding starts to resemble single-channel encoding. Therefore, we also include, in Fig. 10 the reconstruction error of a single-channel TEM, to compare it to the result obtained with two-channel encoding with very small shift.

## VI. CONCLUSION

We have studied multi-channel time encoding of  $2\Omega$ -bandlimited signals, proposed an algorithm for reconstructing an input signal from its samples, and provided sufficient conditions on  $\Omega$  for the algorithm to converge to the correct solution. We have shown that if a TEM machine can perfectly encode a  $2\Omega$ -bandlimited signal, then  $M$  TEMs with the same parameters and with shifts in their integrators can perfectly encode a  $2M\Omega$ -bandlimited signal. The reconstruction algorithm is then based on a projection onto convex sets method.

The improvement on bandwidth that we found is independent of the value of the shifts between the machine integrators, as long as these shifts are nonzero. We have also shown that the knowledge of the relative shifts between the machines is not necessary for reconstruction to be possible. This is not the case in similar setups of multi-channel encoding in the classical sampling scenario where an unknown shift makes the inverse problem more difficult to solve.

## APPENDIX A PREVIOUS RESULTS

**Lemma 8** (Bernstein's inequality). *If  $x = x(t)$  is a function defined on  $\mathbb{R}$  bandlimited to  $[-\Omega, \Omega]$  then  $dx/du$  is also bandlimited and*

$$\left\| \frac{dx}{du} \right\| \leq \Omega \|x\|. \quad (31)$$



Fig. 10: Reconstruction error plotted as a function of bandwidth and integrator shift. A hundred  $2\Omega$ -bandlimited signals, where  $\Omega$  varies between  $\pi/4$  and  $16\pi$  are generated and subsequently sampled and reconstructed using two-channel time encoding and decoding. The TEM used has fixed parameters  $\kappa$ ,  $\delta$  and  $b$  but variable integrator shifts. The mean-squared error is averaged over the hundred randomly generated signals and plotted as a function of bandwidth and shift. Although we have shown that the value of the integrator shifts should have no effect on the reconstructible bandwidth (23), very small shifts perform less well than shifts that are within the same order of magnitude as the threshold  $\delta$ . The rightmost column, separated by the dashed yellow line, shows the reconstruction error when a shift of zero is used. In other words, this is the reconstruction error when using single-channel time encoding and decoding.

**Lemma 9** (Wirtinger's inequality). *If  $x, dx/dt \in L^2(a, b)$  and either  $x(a) = 0$  or  $x(b) = 0$ , then<sup>4</sup>*

$$\int_a^b |x(u)|^2 du \leq \frac{4}{\pi^2} (b-a)^2 \int_a^b \left| \frac{dx}{du} \right|^2 du. \quad (32)$$

**Definition 7.** A set  $\{t_k, k \in \mathbb{Z}\}$  is called *relatively separated* if it can be divided into a finite number of subsets so that  $|x_n - x_m| \geq \beta > 0$  for a fixed  $\beta > 0$ ,  $n \neq m$ , and  $x_n, x_m$  in the same subset.

## APPENDIX B PROOFS

*Proof of Lemma 1:* First, we show that  $\mathcal{P}_\Omega$  is idempotent. Denoting  $G(\omega)$  to be the Fourier transform of  $g(t)$ , we get  $G(\omega) = 1, \forall |\omega| \leq \Omega$  and zero otherwise.

Then,

$$\mathcal{P}_\Omega(\mathcal{P}_\Omega y(t)) = y(t) * g(t) * g(t) = y(t) * g(t), \quad (33)$$

<sup>4</sup>A signal  $x(t)$  is in  $L^2(a, b)$  if  $\|x(t)\|_2 = \left( \int_a^b |x(u)|^2 du \right)^{1/2} < \infty$ .

since  $G(\omega)^2 = G(\omega)$ , so that  $g(t) * g(t) = g(t)$ .

We now show that  $\mathcal{P}_\Omega$  has as range the space of  $2\Omega$ -bandlimited functions. Let  $y(t)$  be a  $2\Omega$ -bandlimited function, then its Fourier transform  $Y(\omega)$  is such that  $Y(\omega) = 0, \forall |\omega| > \Omega$ . Convolution of  $y(t)$  with  $g(t)$  in the time domain only multiplies  $Y(\omega)$  by 1 in the region where it is nonzero. Therefore  $y(t) * g(t) = y(t), \forall y(t)$   $2\Omega$ -bandlimited. ■

*Proof of Lemma 2:* Let  $y_1(t)$  and  $y_2(t)$  be in  $\mathcal{C}_\Omega$ . Then let  $y_3(t)$  be any convex combination of  $y_1(t)$  and  $y_2(t)$ , i.e.  $y_3(t) = \lambda y_1(t) + (1 - \lambda)y_2(t)$ , where  $\lambda \in [0, 1]$ . Then, let  $Y_1(\omega), Y_2(\omega)$  and  $Y_3(\omega)$  be the Fourier transforms of  $y_1(t), y_2(t)$  and  $y_3(t)$  respectively. By linearity of the Fourier transform, we find that  $Y_3(\omega) = \lambda Y_1(\omega) + (1 - \lambda)Y_2(\omega), \forall \omega \in \mathbb{R}$ . Therefore, since  $y_1(t)$  and  $y_2(t)$  are in  $\mathcal{C}_\Omega$  and  $Y_1(\omega) = Y_2(\omega) = 0 \forall |\omega| > \Omega, Y_3(\omega) = 0 \forall |\omega| > \Omega$ . Therefore,  $y_3(t)$  is also in  $\mathcal{C}_\Omega$ . ■

*Proof of Lemma 3:* First we show that  $\mathcal{P}_{A_1}$  is idempotent. Note that  $\int_{t_k}^{t_{k+1}} \mathcal{P}_{A_1} y(u) du = \int_{t_k}^{t_{k+1}} x(u) du, \forall k \in \mathbb{Z}$ . Therefore,

$$\begin{aligned} \mathcal{P}_{A_1}(\mathcal{P}_{A_1} y(t)) &= \mathcal{P}_{A_1} y(t) \\ &+ \sum_{k \in \mathbb{Z}} \int_{t_k}^{t_{k+1}} [x(u) - \mathcal{P}_{A_1} y(u)] du \delta(t - s_k) \\ &= \mathcal{P}_{A_1} y(t). \end{aligned} \quad (34)$$

Now we show that the range of  $\mathcal{P}_{A_1}$  is indeed the space of functions  $y(t)$  with  $\int_{t_k}^{t_{k+1}} y(u) du = \int_{t_k}^{t_{k+1}} x(u) du$ . let  $y_1(t)$  be in this space, then

$$\begin{aligned} \mathcal{P}_{A_1} y_1(t) &= y_1(t) + \sum_{k \in \mathbb{Z}} \int_{t_k}^{t_{k+1}} [x(u) - y_1(u)] du \delta(t - s_k) \\ &= y_1(t) + \sum_{k \in \mathbb{Z}} 0 \times \delta(t - s_k) \\ &= y_1(t) \end{aligned}$$

*Proof of Lemma 4:* Let  $y_1(t)$  and  $y_2(t)$  be in  $\mathcal{C}_{A_1}$ . Then let  $y_3(t)$  be any convex combination of  $y_1(t)$  and  $y_2(t)$ , i.e.  $y_3(t) = \lambda y_1(t) + (1 - \lambda)y_2(t)$ , where  $\lambda \in [0, 1]$ . Then, we have:

$$\begin{aligned} \int_{t_k}^{t_{k+1}} y_3(t) dt &= \int_{t_k}^{t_{k+1}} \lambda y_1(t) + (1 - \lambda)y_2(t) dt \\ &= \lambda \int_{t_k}^{t_{k+1}} y_1(t) dt + (1 - \lambda) \int_{t_k}^{t_{k+1}} y_2(t) dt \\ &= \lambda \int_{t_k}^{t_{k+1}} x(t) dt + (1 - \lambda) \int_{t_k}^{t_{k+1}} x(t) dt \\ &= \int_{t_k}^{t_{k+1}} x(t) dt \end{aligned}$$

The first equality holds because of the definition of  $y_3(t)$ , the second equality holds because  $y_1(t)$  and  $y_2(t)$  are in  $\mathcal{C}_{A_1}$ . The

result shows that  $y_3(t)$  is also in  $\mathcal{C}_{A_1}$ , proving that  $\mathcal{C}_{A_1}$  is a convex set. ■

**Lemma 10.** Assume we have an  $M$ -channel TEM with parameters  $\kappa$ ,  $\delta$  and  $b$ , with shifts  $\alpha_i \neq 0, i = 1 \dots M$ , and input  $x(t)$  such that  $|x(t)| \leq c < b$ . Let  $\{\tilde{t}_k, k \in \mathbb{Z}\}$  be the spike times generated by this  $M$ -channel TEM. In other words,  $\{\tilde{t}_k, k \in \mathbb{Z}\}$  is the combined and ordered set of spike times generated by all channels of the TEM  $A_1, A_2, \dots, A_M$ . Then, the spike times  $\{\tilde{t}_k, k \in \mathbb{Z}\}$  are relatively separated (see Definition 7 in Appendix A).

*Proof:* Assume, without loss of generality that the channels  $A_1, A_2, \dots, A_M$  are ordered by spike time:

$$\begin{aligned} t_k^{(i)} &< t_k^{(i+1)} \quad \forall i = 1 \dots M-1, \\ t_k^{(M)} &< t_{k+1}^{(1)}. \end{aligned}$$

If we denote, as in definition 4,  $\alpha_i, i = 1 \dots M$  to be the shifts between two consecutively spiking machines, then a pair of consecutive spike times  $\tilde{t}_k$  and  $\tilde{t}_{k+1}$  will satisfy

$$\int_{\tilde{t}_k}^{\tilde{t}_{k+1}} x(u) du = 2\kappa\alpha_i - b(t_{k+1} - t_k),$$

for some  $\alpha_i$  that depends on the provenance of  $\tilde{t}_k$  and  $\tilde{t}_{k+1}$ , which is determined by  $k$  since different machines always spike in order (see definition 4).

Now recall that  $|x(t)| \leq c$ , which, when substituted into (35), yields

$$\begin{aligned} c(\tilde{t}_{k+1} - \tilde{t}_k) &\geq 2\kappa\alpha_i - b(\tilde{t}_{k+1} - \tilde{t}_k), \\ \tilde{t}_{k+1} - \tilde{t}_k &\geq \frac{2\kappa\alpha_i}{b+c}, \end{aligned}$$

for some  $i \in \{1, \dots, M\}$  which depends on  $k$ . Then,

$$\tilde{t}_{k+1} - \tilde{t}_k \geq \frac{2\kappa \min_i(\alpha_i)}{b+c},$$

Now denote  $\beta = 2\kappa \min_i(\alpha_i)/(b+c)$ . Note that  $\beta$  is nonzero because all  $\alpha_i$ 's are assumed to be nonzero. Therefore, our sampling set  $\{\tilde{t}_k, k \in \mathbb{Z}\}$  is relatively separated. ■

#### ACKNOWLEDGEMENTS

The authors would like to thank Ivan Dokmanić and Michalina Pacholska for the fruitful discussions.

#### REFERENCES

- [1] A. A. Lazar and L. T. Tóth, "Perfect recovery and sensitivity analysis of time encoded bandlimited signals," *IEEE Transactions on Circuits and Systems I: Regular Papers*, vol. 51, no. 10, pp. 2060–2073, 2004.
- [2] C. E. Shannon, "Communication in the presence of noise," *Proceedings of the IRE*, vol. 37, no. 1, pp. 10–21, 1949.
- [3] M. Vetterli, J. Kovačević, and V. K. Goyal, *Foundations of signal processing*. Cambridge University Press, 2014.
- [4] H. G. Feichtinger and K. Gröchenig, "Theory and practice of irregular sampling," *Wavelets: Mathematics and Applications*, vol. 1994, pp. 305–363, 1994.
- [5] S. Jaffard, "A density criterion for frames of complex exponentials," *The Michigan Mathematical Journal*, vol. 38, no. 3, pp. 339–348, 1991.
- [6] G. Elhami, M. Pacholska, B. B. Haro, M. Vetterli, and A. Scholefield, "Sampling at unknown locations: Uniqueness and reconstruction under constraints," *IEEE Transactions on Signal Processing*, vol. 66, no. 22, pp. 5862–5874, Nov 2018.
- [7] A. Kumar, "On bandlimited signal reconstruction from the distribution of unknown sampling locations," *IEEE Transactions on Signal Processing*, vol. 63, no. 5, pp. 1259–1267, 2015.
- [8] M. Unser, "Sampling – 50 years after shannon," *Proceedings of the IEEE*, vol. 88, no. 4, pp. 569–587, 2000.
- [9] M. Vetterli, P. Marziliano, and T. Blu, "Sampling signals with finite rate of innovation," *IEEE Transactions on Signal Processing*, vol. 50, no. 6, pp. 1417–1428, 2002.
- [10] H. Pan, T. Blu, and M. Vetterli, "Towards generalized FRI sampling with an application to source resolution in radioastronomy," *IEEE Transactions on Signal Processing*, vol. 65, no. 4, pp. 821–835, 2017.
- [11] A. A. Lazar, "Multichannel time encoding with integrate-and-fire neurons," *Neurocomputing*, vol. 65, pp. 401–407, 2005.
- [12] —, "Population encoding with hodgkin-huxley neurons," *IEEE Transactions on Information Theory/Professional Technical Group on Information Theory*, vol. 56, no. 2, 2010.
- [13] W. Maass, "Networks of spiking neurons: the third generation of neural network models," *Neural Networks*, vol. 10, no. 9, pp. 1659–1671, 1997.
- [14] M. Davies, N. Srinivasa, T.-H. Lin, G. Chinya, Y. Cao, S. H. Choday, G. Dimou, P. Joshi, N. Imam, S. Jain *et al.*, "Loihi: a neuromorphic manycore processor with on-chip learning," *IEEE Micro*, vol. 38, no. 1, pp. 82–99, 2018.
- [15] M. Rastogi, A. S. Alvarado, J. G. Harris, and J. C. Principe, "Integrate and fire circuit as an adc replacement," in *2011 IEEE International Symposium of Circuits and Systems (ISCAS)*. IEEE, 2011, pp. 2421–2424.
- [16] S. Saxena and M. Dahleh, "Analyzing the effect of an integrate and fire encoder and decoder in feedback," in *53rd IEEE Conference on Decision and Control*. IEEE, 2014, pp. 3821–3828.
- [17] R. Alexandru and P. L. Dragotti, "Reconstructing classes of non-bandlimited signals from time encoded information," *arXiv preprint arXiv:1905.03183*, 2019.
- [18] A. N. Burkitt, "A review of the integrate-and-fire neuron model: I. homogeneous synaptic input," *Biological Cybernetics*, vol. 95, no. 1, pp. 1–19, 2006.
- [19] D. F. Goodman and R. Brette, "The brian simulator," *Frontiers in Neuroscience*, vol. 3, p. 26, 2009.
- [20] A. Papoulis, "Generalized sampling expansion," *IEEE Transactions on Circuits and Systems*, vol. 24, no. 11, pp. 652–654, 1977.
- [21] A. A. Lazar and E. A. Pnevmatikakis, "Faithful representation of stimuli with a population of integrate-and-fire neurons," *Neural Computation*, vol. 20, no. 11, pp. 2715–2744, 2008.
- [22] K. Adam, A. Scholefield, and M. Vetterli, "Multi-channel time encoding for improved reconstruction of bandlimited signals," in *IEEE International Conference on Acoustics, Speech and Signal Processing (ICASSP)*. IEEE, 2019, pp. 7963–7967.
- [23] A. A. Lazar, "Time encoding with an integrate-and-fire neuron with a refractory period," *Neurocomputing*, vol. 58, pp. 53–58, 2004.
- [24] D. Gontier and M. Vetterli, "Sampling based on timing: Time encoding machines on shift-invariant subspaces," *Applied and Computational Harmonic Analysis*, vol. 36, no. 1, pp. 63–78, 2014.
- [25] W. Cheney and A. A. Goldstein, "Proximity maps for convex sets," *Proceedings of the American Mathematical Society*, vol. 10, no. 3, pp. 448–450, 1959.
- [26] H. H. Bauschke and J. M. Borwein, "On projection algorithms for solving convex feasibility problems," *SIAM Review*, vol. 38, no. 3, pp. 367–426, 1996.

- [27] A. Papoulis, "A new algorithm in spectral analysis and band-limited extrapolation," *IEEE Transactions on Circuits and systems*, vol. 22, no. 9, pp. 735–742, 1975.